PHYSICS

Distinct signature of local tetrahedral ordering in the scattering function of covalent liquids and glasses

Rui Shi and Hajime Tanaka*

Tetrahedral amorphous materials such as SiO_2, GeO_2, Si, Ge, C, and chalcogenides are extremely important in nature and technology. It is known that covalent bonding favors local tetrahedral order in these materials. However, how to extract information on this structural order from the scattering function has remained elusive. By analyzing the structure of simulated SiO_2 and experimental data of various tetrahedral materials, we show that the lowest wave number peak, known as the first sharp diffraction peak (FSDP), and a few higher wave number ones in the scattering functions come from the characteristic density waves of a single tetrahedral unit. FSDP is thus a direct measure of the tetrahedrality. This finding opens the door for long-awaited experimental access to the characterization of disordered amorphous structures.

INTRODUCTION

X-ray and neutron scattering techniques have had great success in the structural determination of crystals. For liquids and amorphous states, they are less powerful than for crystals but are still very useful tools. Because of the macroscopic isotropy and homogeneity, the structure factor $S(\mathbf{k})$ has no angular dependence and is thus a function of only the (scalar) wave number k. $S(k)$ of disordered systems interacting with spherically symmetric potentials are usually featureless and are characterized by a broad amorphous peak around the wave number corresponding to the interatomic distance. This makes the structural analysis of liquids and glasses extremely difficult. For example, the dynamics of a liquid slow down markedly toward the glass transition temperature despite the absence of a clear signature in $S(k)$. This apparent disconnection between structure and dynamics is widely regarded as the main source of difficulty in the understanding of slow glassy dynamics.

However, we show below that this may not be the case for so-called tetrahedral glass-formers. A wide class of materials, such as oxides (*1*–*3*), halides (*4*), chalcogenides (*4*, *5*), monatomic amorphous solids (*6*, *7*), metallic glasses (*8*, *9*), and metal-organic frameworks (*10*, *11*), exhibit a distinct peak in $S(k)$ at a wave number lower than that corresponding to the interparticle distance. This peak is widely known as the first sharp diffraction peak (FSDP). At this moment, the origin of FSDP is a matter of debate (see below). Here, we reveal its structural origin and show that this FSDP provides us with crucial information on structural ordering in the apparently disordered liquid and glass states of tetrahedral materials.

Many models have been proposed to explain FSDP in terms of the underlying atomic structures (*12*). The existing explanations can be categorized mainly into three groups. The first scenario ascribes it to a particular type of structures, i.e., layered (*13*, *14*) or cage-like (*15*) structures, with a spacing larger than the interatomic distance. This interpretation may work for a particular material but cannot be generally applied to, e.g., tetrahedral materials, which can form a three-dimensional (3D) corner-sharing network, a pseudo 1D edge-sharing chain, or a mixture of both (*16*). The second scenario ascribes FSDP to crystal-like structures. In several types of glasses and liquids, it was found that the FSDP position k_1 is close to the first peak in the corresponding crystal structure (*17*, *18*). For example, in SiO_2, $k_1 \approx 2\pi/d_{111}$, where d_{111} is the distance between {111} planes in β-cristobalite. This type of explanation is, however, at odds with the observation that FSDP even appears in the equilibrium liquid state above the melting point, where crystal-like structures can hardly survive.

Last, the third compelling explanation, which was proposed by Blétry (*19*) and Elliott (*20*), attributes FSDP observed in AB_2-type tetrahedral materials to a chemical order originating from the clustering of voids around cations in terms of concentration-concentration partial structure factors in the Bhatia-Thornton formalism (*21*). The peak wave number of FSDP was evaluated from the close packing of binary spheres with chemical orderas follows (*19*, *20*):

$$k_1 = 3\pi/2r \quad (1)$$

where r is the nearest-neighbor cation-cation distance. It was claimed that this formula reasonably predicts the FSDP position for AB_2-type tetrahedral materials (*19*, *20*). However, this scenario was challenged later by a first-principle molecular dynamics simulation of liquid $GeSe_2$ (*22*) and classical molecular dynamics simulations of a polarizable tetrahedral liquid model (*23*), which showed that the appearance of FSDP is not directly linked to this chemical order. Moreover, neutron and x-ray scattering experiments of vitreous SiO_2 reported that the concentration-concentration partial structure factor exhibits no peak in the FSDP position (*24*), providing strong evidence against the chemical-order scenario.

As briefly reviewed above, there has been no consensus on the origin of FSDP despite decades of intensive theoretical and experimental research studies. Moreover, it remains unclear whether there is any link between the development of FSDP and material properties. Here, we propose a novel scenario for FSDP that it originates from the electron density distribution characteristic to a locally favored tetrahedral structure (LFTS) in tetrahedral amorphous materials. This scenario, which we call the "tetrahedron model," explains not only FSDP but also other higher wave number peaks and shoulders in the structure factor in terms of the characteristic length scales of a tetrahedral structural unit, i.e., height, length, and width. We confirm the relevance of this tetrahedron model by carefully comparing its predictions with the peak positions of numerically simulated structure factors of an archetype tetrahedral liquid SiO_2 and experimentally measured structure factors of a wide range of tetrahedral materials. We also show, by molecular dynamics simulation of SiO_2, that the integrated intensity of FSDP is

Department of Fundamental Engineering, Institute of Industrial Science, University of Tokyo, 4-6-1 Komaba, Meguro-ku, Tokyo 153-8505, Japan.
*Corresponding author. Email: tanaka@iis.u-tokyo.ac.jp

directly proportional to the fraction of LFTS or a measure of the degree of local tetrahedral ordering, which was independently estimated by the degree of translational order in the second shell (*25*). Because we showed (*25*) that the fraction of LFTS controls the thermodynamic properties such as the density anomaly of silica (*26*), our finding suggests a strong connection between FSDP and the properties of tetrahedral materials.

RESULTS

The structure factor, which is the density-density correlation in reciprocal space, is given by

$$S(\mathbf{k}) = \frac{1}{N}\langle \rho_{\mathbf{k}}\rho_{-\mathbf{k}}\rangle \quad (2)$$

where N is the number of particles, $\langle \cdots \rangle$ denotes the ensemble average, and $\rho_{\mathbf{k}}$ is the Fourier component of the number density ρ, defined by

$$\rho_{\mathbf{k}} = \sum_{i=1}^{N} \exp(-i\mathbf{k}\cdot\mathbf{r}_i) \quad (3)$$

where $\mathbf{r}_i$ is the position vector of atom i.

Because crystal atoms have a periodic arrangement, density wave $\rho_{\mathbf{k}}$ has well-defined components at particular wave vectors $\mathbf{k}$'s, which produce sharp peaks in the structure factor. On the other hand, the atomic arrangement in a disordered noncrystalline system lacks a long-range translational order, and thus, there are no such sharp peaks unlike the case of a crystal. However, atoms are still arranged in a regular manner locally to lower the free energy. Thus, it is natural to consider that if there is a specific regular arrangement of atoms, then it can have characteristic density waves beyond the nearest interatomic distance, which may produce FSDP in the structure factor. This is our basic idea.

Tetrahedral materials, by definition, tend to locally form tetrahedral unit structures. So we first focus on the characteristics of density waves embedded in a regular tetrahedron, which we show schematically in Fig. 1A. We can see that the tetrahedral unit, whose nearest interatomic distance is r, can be characterized by three key length scales: height H, edge length L, and width D. Here, $H, L, D > r$. The structure factor of an isolated regular tetrahedron (see Fig. 1A) can be straightforwardly calculated from Eqs. 2 and 3 independently along the x, y, and z axes. The analytical solutions are given by eqs. S2 to S4, and the results are displayed in Fig. 1B. We can see that, despite small deviations due to the interference of different peaks, the structure factor $S(k)$ of a regular tetrahedron shows four characteristic peaks in the range of $0.5 \le kr/2\pi \le 2.75$, which originates from the density waves associated with the underlying characteristic lengths, H, L, and D, of a tetrahedron.

We can see in Fig. 1B that the FSDP located at $kr/2\pi \simeq 3/4$ comes mainly from the density wave along the z axis with $k = 2\pi/H$. The second peak at $kr/2\pi \simeq \sqrt{3/2}$ originates from the density wave along the x axis with $k = 4\pi/L$. The third and fourth peaks are at $kr/2\pi \simeq 3\sqrt{2}/2$ and $2\sqrt{3/2}$, which stem from density waves along the y and x axes, with $k = 6\pi/D$ and $8\pi/L$, respectively. The separation between these two peak positions is very small. Some other signals also exist but are substantially smaller and thus may not be observed as clear peaks. We summarize the characteristic peak positions for a regular tetrahedron in Table 1. Here, it is worth noting that our tetrahedron model predicts exactly the same FSDP location at $k_1 = 3\pi/2r$, proposed as Blétry and Elliott's close-packed binary spheres model (see Eq. 1) (*19*, *20*). However, we emphasize that the physical mechanism is essentially different between the two models. The FSDP in our model originates from the density waves generated by a tetrahedral unit that is common to all tetrahedral materials. However, their model ascribes FSDP to the chemical order of close-packed binary spheres, whose relevance to tetrahedral materials characterized by low coordination is questionable.

Recently, by introducing a new structural descriptor z that characterizes the translational order in the second shell, we revealed that liquid silica can be physically treated as a dynamical mixture of two types of local structures (or two states) (*27*), which was verified by a bimodal distribution of z (*25*) in molecular dynamics simulations of silica with the van Beest, Kramer, and van Santen (BKS) empirical potential (*28*). At a high temperature, silica mainly consists of disordered normal-liquid structures, whereas upon cooling more and more LFTSs with high translational and tetrahedral orders are formed in the sea disordered normal-liquid structures. We showed by simulations that this two-state model can naturally explain the density anomaly of silica (*25*).

In our model, FSDP is explained by the formation of LFTS and the resulting unique density waves characteristic to a tetrahedron. On the other hand, our structural descriptor z also detects the same LFTS by focusing on the translational order of the second shell, which is a consequence of the formation of a regular tetrahedral structure protected from invasion of other atoms. Thus, it is quite natural to expect a close

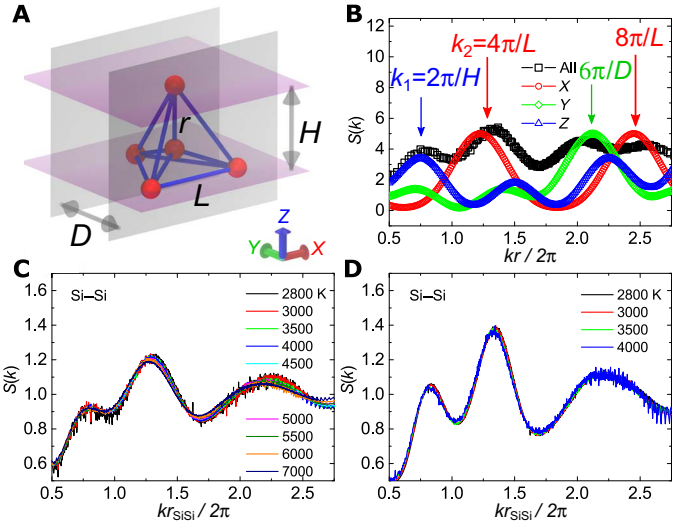

Fig. 1. Structure factor of an isolated LFTS. (**A**) Regular tetrahedron with the nearest interatomic distance r, height H, edge length L, and width D. (**B**) Structure factor $S(k)$ of the regular tetrahedron in the x, y, and z directions [see (A) for the definitions of the directions] together with that averaged over all orientations (black square, multiplied by a factor of 4). Arrows in (B) indicate the locations of four characteristic peaks. (**C**) Si–Si partial structure factor of a typical LFTS, $SiSi_4$ (central Si and its four neighboring Si in the first shell). (**D**) Si–Si partial structure factor of a cluster of typical LFTS, $SiSi_{16}$ (central Si and its 16 neighboring Si up to the second shell). The structure factors of the cluster at $T > 4000$ K are not shown, because at these high temperatures there are few LFTSs forming these clusters. Here, a typical LFTS is selected by imposing the following three criteria on a central Si: (i) the structural descriptor $2.4 \le z \le 2.6$ Å, (ii) four Si neighbors in its first shell, and (iii) the tetrahedral order parameter $q \ge 0.8$ (see Materials and Methods for the definitions of z and q).

Table 1. Geometric parameters characterizing a regular tetrahedron and the corresponding characteristic wave numbers. See Fig. 1A for the definition of the parameters.

Geometric parameter	Relation with r in real space	Peak position k in reciprocal space	Scaled primary peak position $kr/2\pi$
L	$\sqrt{8/3}r$	$4\pi/L = \sqrt{6}\pi/r$	$\sqrt{3/2}$
D	$\sqrt{2}r$	$6\pi/D = 3\sqrt{2}\pi/r$	$3\sqrt{2}/2$
H	$4r/3$	$2\pi/H = 3\pi/2r$	$3/4$

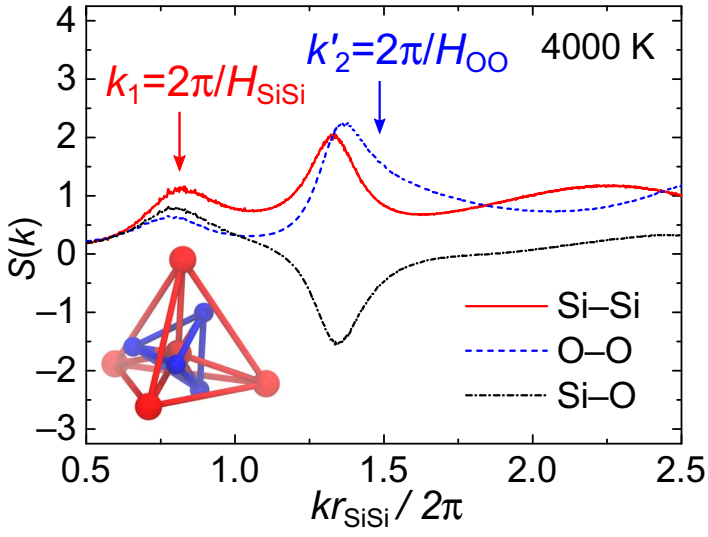

Fig. 2. The Si–Si, O–O, and Si–O partial structure factors at 1 bar and 4000 K. The FSDP (red arrow) in the structure factor corresponds to the height H_{SiSi} of the silicon tetrahedron, $k_1 = 2\pi/H_{SiSi}$. The shoulder (blue arrow) near the second peak of the O–O structure factor corresponds to the height H_{OO} of the oxygen tetrahedron, $k_2^{'} = 2\pi/H_{OO}$. The inset shows two regular tetrahedra sharing one center Si. Red and blue spheres denote Si and O atoms, respectively.

connection between FSDP and LFTS. Here, we directly check this hypothesis by looking at the Si–Si partial structure factor of a typical LFTS, $SiSi_4$ (averaged over random locations and orientations) in liquid silica by simulations. As shown in Fig. 1C, the structure factor exhibits the three characteristic peaks in the range $0.5 \leq kr_{SiSi}/2\pi \leq 2.5$, which are predicted by our tetrahedron model (Fig. 1B). Here, r_{SiSi} denotes the first peak position in the Si–Si radial distribution function. The third and fourth peaks for a regular tetrahedron merge into a broad peak at $kr_{SiSi}/2\pi \sim 2.25$ for liquid silica. Here, we note that the emergence of FSDP is linked to the high local tetrahedral order and its peak height is positively correlated with the degree of tetrahedral order (see fig. S2).

Next, we show the Si–Si structure factor of a cluster of LFTS, $SiSi_{16}$, including a central Si and its 16 Si neighbors up to the second shell (averaged over random positions and orientations) in Fig. 1D. Compared to an isolated LFTS (Fig. 1C), we can see that the peaks become narrower and higher, indicating the increase in the coherence length due to a coherent spatial arrangement of neighboring tetrahedra. This is supported by the increase of the coherence length, which is estimated from the width of FSDP, from ~1.8 Å in Fig. 1C to ~2.5 Å in Fig. 1D (see Supplementary Text for details). We note that this coherence mainly comes from the local development of the translational order, but not from that of the orientational order. This short coherence length is consistent with our previous finding that orientational order basically does not extend beyond the first shell in silica, which is an origin of silica's much higher glass-forming ability compared to water despite both having similar translational orders (*25*). Moreover, we confirm that the integrated intensities (obtained by fitting three Lorentzian peaks) of FSDP in Fig. 1 (C and D) are almost the same, supporting the proportionality between the FSDP-integrated intensity and the number of atoms involved in LFTSs. Later, we will show for silica that the integrated intensity of FSDP is a direct measure of the fraction of LFTS or the degree of local structural ordering.

Tetrahedral materials of AB_2 type can be generally categorized into two groups in terms of preferential arrangements of tetrahedrons, corner-sharing and edge-sharing groups, depending on the connectivity of neighboring AB_4 tetrahedral units. It is known that, for the former, the 3D tetrahedral network tends to be formed, whereas for the latter, pseudo 1D chain-like structures tend to develop (*16*). SiO_2 is known as a typical corner-sharing tetrahedral material, and as a result, two types of tetrahedra are formed locally: a small oxygen tetrahedron SiO_4 and a large silicon tetrahedron $SiSi_4$ (see the inset of Fig. 2). According to our tetrahedron model, signals from both silicon and oxygen tetrahedra should appear in the structure factor.

Figure 2 shows the partial structure factors of liquid silica at 1 bar and 4000 K. It can be seen that, beside FSDP at $kr_{SiSi}/2\pi \simeq 3/4$, which is observed for all the partial structure factors, a clear shoulder appears at $kr_{SiSi}/2\pi \simeq 3/2$ only for the O–O partial structure factor. We note that this shoulder is observed in the O–O partial structure

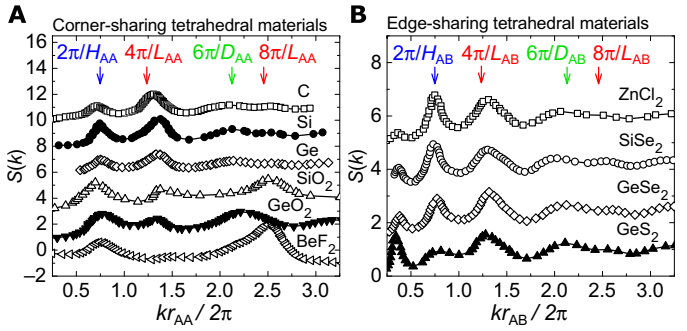

Fig. 3. Experimental structure factors of various tetrahedral materials. (**A**) Structure factors $S(k)$ of corner-sharing tetrahedral materials [monatomic A=C (*34*), Si (*35*), and Ge (*36*) and binary AB_2=SiO_2 (*24*), GeO_2 (*37*), and BeF_2 (*38*)] as a function of the wave number k scaled by the average A-A distance r_{AA}. (**B**) Structure factors $S(k)$ of edge-sharing tetrahedral materials [binary AB_2=$ZnCl_2$ (*39*), $SiSe_2$ (*40*), $GeSe_2$ (*41*), and GeS_2 (*42*)] as a function of the wave number k scaled by the average A-B distance r_{AB}. Peak positions predicted by our tetrahedron model (see Fig. 1B) are shown by arrows. Open and filled symbols denote $S(k)$ measured by neutron and x-ray scattering experiments, respectively. Except for molten $ZnCl_2$, all the materials were measured in the glassy (or amorphous) solid state.

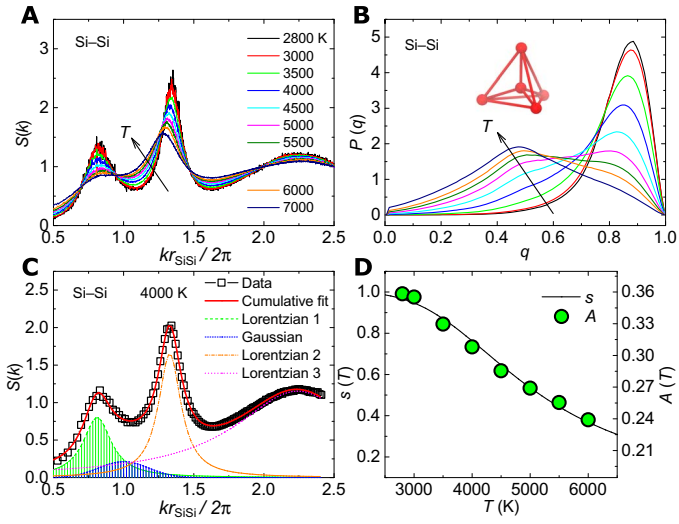

Fig. 4. Local structural ordering as a function of temperature in liquid silica. (**A**) Si–Si partial structure factors at 1 bar for various temperatures. (**B**) Tetrahedral order parameter q for $SiSi_4$ unit at 1 bar for the various temperatures. The tetrahedral order parameter q = 1 for a regular tetrahedron and q = 0 for a random configuration (see Eq. 4 for the definition). Arrows in (A) and (B) denote the direction of the temperature increase. (**C**) Decomposition of the Si–Si partial structure factor at 4000 K by three Lorentzian functions and one Gaussian function. (**D**) The integrated intensity, A, of FSDP [green area in (C)] is a good measure of the fraction s of LFTS, which controls the density anomaly of liquid silica (*25*).

factor at all temperatures we studied. Given the relation $r_{SiSi} \simeq 2r_{SiO}$, the shoulder location can be estimated as $kr_{SiO}/2\pi \simeq 3/4$ after scaling by the average Si–O distance r_{SiO}, which in our tetrahedron model corresponds to the density wave along the height H_{OO} of an oxygen tetrahedron SiO_4. We can also see this shoulder in the experimental structure factor of glassy silica obtained by neutron scattering (see Fig. 3A). This appearance of a shoulder at $kr_{SiO}/2\pi \simeq 3/4$ in the O–O partial structure factor further supports the relevance of our tetrahedron model for tetrahedral materials.

It is natural to expect that our tetrahedron model, based on the density waves characteristic to a single tetrahedral unit, should be valid for all tetrahedral materials. To further check the generality of our tetrahedron model, we collected experimental structure factors of various types of tetrahedral materials, including oxides, halides, chalcogenides, and monoatomic amorphous materials, measured by x-ray and neutron scatterings, and show them in Fig. 3. We categorize these materials (denoted as monatomic A and binary AB_2) into corner-sharing (Fig. 3A) and edge-sharing (Fig. 3B) groups (*16*). The largest tetrahedron unit is AA_4 and AB_4 for the corner-sharing and edge-sharing tetrahedral materials, respectively. Therefore, we scale the structure factors by the average A-A distance r_{AA} for the corner-sharing group and by the average A-B distance r_{AB} for the edge-sharing one. As seen in Fig. 3, four characteristic peaks (or shoulders, e.g., $k = 6\pi/D_{AA}$ for SiO_2 and BeF_2) generally appear at the locations expected for a regular tetrahedron, strongly supporting our tetrahedron model. We note that small deviations may come from distortions of tetrahedral units under thermal fluctuations. For the edge-sharing group, we can also see a distinct low k peak corresponding to a length scale larger than H_{AB}, which is observed as the first peak in Fig. 3B. We speculate that this peak stems from some other structure (e.g., chain-like structure) extending beyond H_{AB}, but the underlying structure behind this peak might be material specific. Further study is necessary to elucidate its structural origin.

DISCUSSION

Until now, we have shown that the characteristic features, including FSDP, of the structure factors of a wide class of tetrahedral materials can be well explained by our simple tetrahedron model. Then, the remaining question is what kind of information on tetrahedral materials can our model provide from the behavior of the structure factor, particularly the behavior of FSDP. To answer this question, we systematically study the temperature dependence of the structure factor of liquid silica by simulations. As shown in Fig. 4A, FSDP continuously grows upon cooling, indicating a rapid increase of the number density of LFTS. This is consistent with the increase of the tetrahedral order for the $SiSi_4$ unit upon cooling (see Fig. 4B).

The degree of local structural ordering in liquid silica can be described by a two-state model (*27*), where the system is effectively treated as a dynamical mixture of LFTS and disordered normal-liquid structures (*25*). The former produces FSDP, whereas the latter gives rise to a broad peak at $k \simeq 2\pi/r_{SiSi}$, or $kr_{SiSi}/2\pi \simeq 1$, as typically observed in simple liquids such as hard spheres or Lennard-Jones liquids. The emergence of a peak around $kr_{SiSi}/2\pi \simeq 1$ can be seen in the structure factors at high pressures (see fig. S1), where liquid silica predominantly consists of disordered normal-liquid structures because LFTS costs an extra volume and is thus not favored at high pressures.

On the basis of this consideration, we find that the structure factors at all the temperatures we studied can be well fitted by three Lorentzian functions related to tetrahedral structures and one Gaussian function specifically associated with disordered normal-liquid structures, whose peak position is fixed at $kr_{SiSi}/2\pi = 1$ (see eq. S1). The fitting result at 4000 K is shown in Fig. 4C. We note that the fittings at other temperatures (not shown) have similar quality. Here, the green peak (FSDP) originates purely from LFTS, and thus, its integrated intensity should be proportional to the fraction of LFTS. This is confirmed in Fig. 4D, where we compare the integrated intensity A of FSDP (green area in Fig. 4C) and the fraction s of LFTS as a function of temperature at 1 bar in liquid silica. The fraction s was independently determined by a

structural descriptor z (*25*) that measures local translational order in SiO_2. The integrated intensity of FSDP is an excellent measure of the fraction of LFTS or the degree of local structural ordering. Note that tetrahedral ordering is usually associated with local translational ordering and is thus linked to local density, energy, and entropy (*27*). For example, as we showed in our previous paper (*25*), the fraction s, which is an order parameter in the two-state model (*27*), controls the density anomaly of liquid silica through its direct link to the volume difference between LFTS and normal-liquid structures. Therefore, we may conclude that FSDP is a key structural feature controlling the thermodynamic properties of silica, implying that FSDP may serve as a general structural descriptor in the characterization of a wide class of materials with tetrahedral coordination. We find that the temperature dependence of the local structural ordering signaled by FSDP is consistent with the two-state prediction for SiO_2, but its relevance to other materials should be examined carefully in the future.

To summarize, we have proposed a novel interpretation of FSDP commonly observed in tetrahedral materials: FSDP is a direct consequence of the density waves characteristic to LFTS spontaneously formed in tetrahedral materials at relatively low temperature and pressure. Our tetrahedron model, which relies on neither the crystal-like structure (cluster) nor the chemical-ordered binary spheres, explains the structural origin of not only FSDP but also the other characteristic higher wave number peaks and shoulders in the structure factors of a wide class of tetrahedral materials. We stress that FSDP is a structural indicator of local structural ordering in disordered liquids and amorphous solids. We can directly estimate the degree and range of local structural ordering quantitatively from the integrated intensity and width of FSDP measured by scattering experiments without any assumption. This allows long-awaited experimental access to a link between the structure and the physical properties of disordered noncrystalline materials including thermal, mechanical, optical, and dynamic properties. We hope that our finding will greatly advance our understanding of tetrahedral materials such as SiO_2, GeO_2, Si, Ge, C, and chalcogenides, which are of significant importance in materials science, industrial applications, and geology. Last, we argue that the structural origin of FSDP reported here may be generally relevant to disordered materials with FSDP, such as metallic systems having a tendency to form icosahedral structures.

MATERIALS AND METHODS

Simulation methods

Molecular dynamics simulations were carried out in a cubic box containing 3456 BKS (*28*–*30*) SiO_2 (3456 silicon and 6912 oxygen atoms) by using the LAMMPS (*31*) package. Periodic boundary conditions were applied in all directions. Intermolecular interactions were truncated at 5.5 Å, and long-range Coulomb interactions were treated by a particle-particle particle-mesh method. All simulations were performed in the constant-temperature, constant-pressure (NPT) ensemble. The temperature and pressure were kept constant by using the Nosé-Hoover thermostat and barostat, respectively. A time step of 1 fs was used in all the simulations below 6000 K. Above 6000 K, the time step was adjusted to 0.5 fs to avoid overlap of atoms within one step. More simulation details can be found in (*25*).

Microscopic structural descriptors

In our recent study (*25*), we proposed a new structural descriptor z to measure the translational order in silicon's second shell. z is defined for each Si atom i as the difference between the distance d_{ji} of the fifth nearest Si neighbor j and the distance $d_{j'i}$ of the fourth nearest O neighbor j': $z(i) = d_{ji} - d_{j'i}$. By measuring the relative distance between the first and second shells of silicon, z characterizes the translational order of silicon's second shell. The distribution of z shows a clear bimodal feature, supporting the existence of two states in liquid SiO_2 (*25*).

The tetrahedral order in the first shell was also evaluated for a silicon atom by using the parameter q that is defined by (*32*, *33*)

$$q = 1 - \frac{3}{8}\sum_{i=1}^{3}\sum_{j=i+1}^{4}\left(\cos\phi_{ij} + \frac{1}{3}\right)^2 \quad (4)$$

where ϕ_{ij} is the angle formed by two vectors pointing from the center silicon to two of its neighboring silicon atoms. The summation runs over all the combinations of the four nearest neighbors.

SUPPLEMENTARY MATERIALS

Supplementary material for this article is available at http://advances.sciencemag.org/cgi/content/full/5/3/eaav3194/DC1

Supplementary Text

Fig. S1. Si–Si partial structure factors at 5000 K and various pressures.

Fig. S2. Relationship between the structure factor $S(k)$ and the tetrahedral order parameter q at 1 bar and 4000 K.

REFERENCES AND NOTES

1. S. Kohara, J. Akola, H. Morita, K. Suzuya, J. K. R. Weber, M. C. Wilding, C. J. Benmore, Relationship between topological order and glass forming ability in densely packed enstatite and forsterite composition glasses. *Proc. Natl. Acad. Sci. U.S.A.* **108**, 14780–14785 (2011).
2. C. Sanloup, J. W. E. Drewitt, Z. Konôpková, P. Dalladay-Simpson, D. M. Morton, N. Rai, W. van Westrenen, W. Morgenroth, Structural change in molten basalt at deep mantle conditions. *Nature* **503**, 104–107 (2013).
3. S. Kohara, J. Akola, L. Patrikeev, M. Ropo, K. Ohara, M. Itou, A. Fujiwara, J. Yahiro, J. T. Okada, T. Ishikawa, A. Mizuno, A. Masuno, Y. Watanabe, T. Usuki, Atomic and electronic structures of an extremely fragile liquid. *Nat. Commun.* **5**, 5892 (2014).
4. P. S. Salmon, R. A. Martin, P. E. Mason, G. J. Cuello, Topological versus chemical ordering in network glasses at intermediate and extended length scales. *Nature* **435**, 75–78 (2005).
5. W. A. Crichton, M. Mezouar, T. Grande, S. Stølen, A. Grzechnik, Breakdown of intermediate-range order in liquid $GeSe_2$ at high pressure. *Nature* **414**, 622–625 (2001).
6. J. M. Zaug, A. K. Soper, S. M. Clark, Pressure-dependent structures of amorphous red phosphorus and the origin of the first sharp diffraction peaks. *Nat. Mater.* **7**, 890–899 (2008).
7. Z. Zeng, L. Yang, Q. Zeng, H. Lou, H. Sheng, J. Wen, D. J. Miller, Y. Meng, W. Yang, W. L. Mao, H.-k. Mao, Synthesis of quenchable amorphous diamond. *Nat. Commun.* **8**, 322 (2017).
8. D. Ma, A. D. Stoica, X.-L. Wang, Power-law scaling and fractal nature of medium-range order in metallic glasses. *Nat. Mater.* **8**, 30–34 (2009).
9. Q. Luo, G. Garbarino, B. Sun, D. Fan, Y. Zhang, Z. Wang, Y. Sun, J. Jiao, X. Li, P. Li, N. Mattern, J. Eckert, J. Shen, Hierarchical densification and negative thermal expansion in Ce-based metallic glass under high pressure. *Nat. Commun.* **6**, 5703 (2015).
10. T. D. Bennett, D. A. Keen, J.-C. Tan, E. R. Barney, A. L. Goodwin, A. K. Cheetham, Thermal amorphization of zeolitic imidazolate frameworks. *Angew. Chem. Int. Ed.* **50**, 3067–3071 (2011).
11. R. Gaillac, P. Pullumbi, K. A. Beyer, K. W. Chapman, D. A. Keen, T. D. Bennett, F.-X. Coudert, Liquid metal–organic frameworks. *Nat. Mater.* **16**, 1149–1154 (2017).
12. S. R. Elliott, Medium-range structural order in covalent amorphous solids. *Nature* **354**, 445–452 (1991).
13. J. C. Philips, Topology of covalent non-crystalline solids II: Medium-range order in chalcogenide alloys and A-Si (Ge). *J. Non-Cryst. Solids* **43**, 37–77 (1981).
14. L. E. Busse, S. R. Nagel, Temperature dependence of the structure factor of As_2Se_3 glass up to the glass transition. *Phys. Rev. Lett.* **47**, 1848–1851 (1981).
15. A. C. Wright, Neutron scattering from vitreous silica. V. The structure of vitreous silica: What have we learned from 60 years of diffraction studies? *J. Non-Cryst. Solids* **179**, 84–115 (1994).

16. M. Wilson, P. S. Salmon, Network topology and the fragility of tetrahedral glass-forming liquids. *Phys. Rev. Lett.* **103**, 157801 (2009).
17. P. H. Gaskell, D. J. Wallis, Medium-range order in silica, the canonical network glass. *Phys. Rev. Lett.* **76**, 66–69 (1996).
18. J. K. Christie, S. N. Taraskin, S. R. Elliott, Structural characteristics of positionally disordered lattices: Relation to the first sharp diffraction peak in glasses. *Phys. Rev. B* **70**, 134207 (2004).
19. J. Blétry, Sphere and distance models for binary disordered systems. *Philos. Mag. B* **62**, 469–508 (1990).
20. S. R. Elliott, Origin of the first sharp diffraction peak in the structure factor of covalent glasses. *Phys. Rev. Lett.* **67**, 711–714 (1991).
21. A. B. Bhatia, D. E. Thornton, Structural aspects of the electrical resistivity of binary alloys. *Phys. Rev. B* **2**, 3004–3012 (1970).
22. C. Massobrio, A. Pasquarello, Origin of the first sharp diffraction peak in the structure factor of disordered network-forming systems: Layers or voids? *J. Chem. Phys.* **114**, 7976–7979 (2001).
23. M. Wilson, B. K. Sharma, The evolution of intermediate-range order in molten network-forming materials. *J. Chem. Phys.* **128**, 214507 (2008).
24. Q. Mei, C. J. Benmore, S. Sen, R. Sharma, J. L. Yarger, Intermediate range order in vitreous silica from a partial structure factor analysis. *Phys. Rev. B* **78**, 144204 (2008).
25. R. Shi, H. Tanaka, Impact of local symmetry breaking on the physical properties of tetrahedral liquids. *Proc. Natl. Acad. Sci. U.S.A.* **115**, 1980–1985 (2018).
26. C. A. Angell, H. Kanno, Density maxima in high-pressure supercooled water and liquid silicon dioxide. *Science* **193**, 1121–1122 (1976).
27. H. Tanaka, Bond orientational order in liquids: Towards a unified description of water-like anomalies, liquid-liquid transition, glass transition, and crystallization. *Eur. Phys. J. E Soft Matter* **35**, 113 (2012).
28. B. W. H. van Beest, G. J. Kramer, R. A. van Santen, Force fields for silicas and aluminophosphates based on ab initio calculations. *Phys. Rev. Lett.* **64**, 1955–1958 (1990).
29. J. Horbach, W. Kob, Static and dynamic properties of a viscous silica melt. *Phys. Rev. B* **60**, 3169–3181 (1999).
30. I. Saika-Voivod, F. Sciortino, P. H. Poole, Computer simulations of liquid silica: Equation of state and liquid–liquid phase transition. *Phys. Rev. E* **63**, 011202 (2000).
31. S. Plimpton, Fast parallel algorithms for short-range molecular dynamics. *J. Comput. Phys.* **117**, 1–19 (1995).
32. P.-L. Chau, A. J. Hardwick, A new order parameter for tetrahedral configurations. *Mol. Phys.* **93**, 511–518 (1998).
33. J. R. Errington, P. G. Debenedetti, Relationship between structural order and the anomalies of liquid water. *Nature* **409**, 318–321 (2001).
34. K. W. R. Gilkes, P. H. Gaskell, J. Robertson, Comparison of neutron-scattering data for tetrahedral amorphous carbon with structural models. *Phys. Rev. B* **51**, 12303 (1995).
35. K. Laaziri, S. Kycia, S. Roorda, M. Chicoine, J. L. Robertson, J. Wang, S. C. Moss, High-energy x-ray diffraction study of pure amorphous silicon. *Phys. Rev. B* **60**, 13520 (1999).
36. G. Etherington, A. C. Wright, J. T. Wenzel, J. C. Dore, J. H. Clarke, R. N. Sinclair, A neutron diffraction study of the structure of evaporated amorphous germanium. *J. Non-Cryst. Solids* **48**, 265–289 (1982).
37. S. Kohara, K. Suzuya, Intermediate-range order in vitreous SiO_2 and GeO_2. *J. Phys. Condens. Matter* **17**, S77 (2005).
38. A. C. Wright, A. G. Clare, G. Etherington, R. N. Sinclair, S. A. Brawer, M. J. Weber, A neutron diffraction and molecular dynamics investigation of the structure of vitreous beryllium fluoride. *J. Non-Cryst. Solids* **111**, 139–152 (1989).
39. D. A. Allen, R. A. Howe, N. D. Wood, W. S. Howells, Tetrahedral coordination of Zn ions in molten zinc halides. *J. Chem. Phys.* **94**, 5071–5076 (1991).
40. R. W. Johnson, D. L. Price, S. Susman, M. Arai, T. I. Morrison, G. K. Shenoy, The structure of silicon-selenium glasses: I. Short-range order. *J. Non-Cryst. Solids* **83**, 251–271 (1986).
41. S. Susman, K. J. Volin, D. G. Montague, D. L. Price, The structure of vitreous and liquid $GeSe_2$: A neutron diffraction study. *J. Non-Cryst. Solids* **125**, 168–180 (1990).
42. A. Zeidler, J. W. E. Drewitt, P. S. Salmon, A. C. Barnes, W. A. Crichton, S. Klotz, H. E. Fischer, C. J. Benmore, S. Ramos, A. C. Hannon, Establishing the structure of GeS_2 at high pressures and temperatures: A combined approach using x-ray and neutron diffraction. *J. Phys. Condens. Matter* **21**, 474217 (2009).

Acknowledgments
Funding: This study was partly supported by Scientific Research (A) and Specially Promoted Research (KAKENHI grants nos. JP18H03675 and JP25000002, respectively) from the Japan Society for the Promotion of Science (JSPS). **Author contributions:** H.T. proposed and supervised the study. R.S. performed research. R.S and H.T. discussed the results and wrote the manuscript. **Competing interests:** The authors declare that they have no competing interests. **Data and materials availability:** All data needed to evaluate the conclusions in the paper are present in the paper and/or the Supplementary Materials. Additional data related to this paper may be requested from the authors.

Submitted 5 September 2018
Accepted 16 January 2019
Published 1 March 2019
10.1126/sciadv.aav3194

Citation: R. Shi, H. Tanaka, Distinct signature of local tetrahedral ordering in the scattering function of covalent liquids and glasses. *Sci. Adv.* **5**, eaav3194 (2019).

Distinct signature of local tetrahedral ordering in the scattering function of covalent liquids and glasses

Rui Shi and Hajime Tanaka

Sci Adv **5** (3), eaav3194.
DOI: 10.1126/sciadv.aav3194